Research Article | Vol. 28, No. 2 / 20 January 2020 / Optics Express 2156

Optics EXPRESS

Wavelength-dependent orientation of the principal axes of photonic crystal fibers measured by windowed Fourier-transform spectral interferometry

MERCÉDESZ HORVÁTH,[1,*] BÁLINT G. NAGYILLÉS,[1] TÍMEA GRÓSZ,[2] AND ATTILA P. KOVÁCS[1]

[1] Department of Optics and Quantum Electronics, University of Szeged, Dóm tér 9, H-6720 Szeged, Hungary
[2] ELI-ALPS, ELI-HU Non-Profit Ltd., Dugonics tér 13, H-6720 Szeged, Hungary
[*] horvathmercedesz@titan.physx.u-szeged.hu

Abstract: We present a novel polarization alignment technique based on windowed Fourier-transform (WFT) spectral interferometry to determine the wavelength-dependent orientation of the principal polarization axes of photonic crystal fibers (PCFs). To test the technique, a commercially available, 82.5-cm-long HC-800-02 type hollow-core PCF was measured. The angles belonging to the fast and the slow principal axes of the fiber were determined from the peak intensity values of the ridges in the WFT map at different wavelengths. We demonstrate that the orientation of the principal polarization axes of the tested PCF is wavelength-dependent. The precision of the angle measurement was better than 0.3°.

1. Introduction

Polarization maintaining fibers (PMFs) have become widespread in coherent optical communication, optical fiber interferometry and sensing as well. PMFs can only maintain the linear state of the polarization if the linearly polarized light is launched into the fiber along one of its principal axes precisely. Even a small angular misalignment may cause polarization mode dispersion and crosstalk. Therefore, the precise measurement of the orientation of the principal axes is important for every application involving light coupling and fiber splicing procedures.

Several polarization alignment methods have been developed in the last decades for highly birefringent fibers and PMFs. The simplest ones are based on the direct observation of the fiber ends using a microscope [1], a CCD camera [2,3] or a polarization alignment instrument that is specially developed for PANDA type PMFs [4]. There are more precise methods, based on monitoring the change in the phase difference between the polarization modes, which rely on the rotation of the polarization plane of the light beam [5] or the rotation of the fiber itself [6]. Other techniques combine the rotation with external perturbations of the fiber, which are often achieved by heating [7–11], applying transversal stress [12], pressure [13] or with a frequency-tunable laser [14,15]. Interferometric methods employing a Michelson-interferometer [16] or a fiber interferometer [17] are also used especially for alignment during fiber splicing. Comparing the precision of the methods above, we found that the direct observation of the fiber ends usually results in 1° or 2° misalignment. The precision of methods based on monitoring the change in the phase difference varies typically between 0.2° and 1° in the case of those relying on the rotation of the polarization plane or the fiber, while the ones based on the combination of the rotation and perturbations have a precision of 0.1°-0.5°. The most precise technique is the interferometric one with 0.09°.

These methods are suitable for measuring the orientation of the principal axes, nevertheless the majority of these use wavelength-independent detection or only monochromatic light sources, thus the wavelength-dependent orientation of the principal axes has not been investigated by these

#381769 https://doi.org/10.1364/OE.381769
Journal © 2020 Received 6 Nov 2019; revised 11 Dec 2019; accepted 11 Dec 2019; published 15 Jan 2020

Optics EXPRESS

techniques. However, the knowledge of the wavelength-dependent orientation of the principal axes is essential in the ultrafast technology where laser pulses having very broad spectra are sent through birefringent optical fibers. In this case, the simultaneous excitation of the orthogonal polarization modes of the fiber can be induced by the inaccurate angular alignment of the principal axes at different wavelengths of the laser pulses. The effect of dispersive orientation of the principal axes is also important in the telecommunication, where even a small misalignment at a given wavelength can cause crosstalk [7].

Tarnowski et al. fabricated a specially designed side-hole fiber having a tilted elliptical core with a slow axis that had dispersive orientation, meaning that its angle was wavelength-dependent [18]. They also used a polarization alignment technique employing a polarizer and an analyzer and examined its wavelength-dependence with an optical spectrum analyzer. The precision of their measurements was about 1°.

With the appearance of hollow-core photonic crystal fibers (HC-PCFs), it has become possible to modify the fiber structure within certain limits according to the requirements of the application. Nevertheless, slight changes in the structure that affect the optical properties can be expected after manufacturing. Hence, it would be important to develop a precise polarization alignment technique for fiber diagnostic measurements and to examine the wavelength-dependence of the angular position of the polarization axes. Previously, we successfully used the windowed Fourier-transform (WFT) method to measure the chromatic dispersion of a HC-PCF [19].

In this work, we present a new polarization alignment method also based on WFT spectral interferometry, which is suitable for measuring the wavelength-dependence of the orientation of the principal axes of PCFs. The method was tested on a commercially available HC-PCF.

2. Experimental setup

The experimental setup, as depicted in Fig. 1, was based on a combination of a Mach-Zehnder interferometer and a high-resolution spectrometer (spectral range: 710-890 nm, spectral resolution: 0.2 nm). The interferometer was illuminated by a Ti:Sapphire laser oscillator producing pulses of 6 fs at 800 nm, having spectral bandwidth of about 150 nm. A polarizer with vertical transmission axis (P1, spectral range: 650-2000 nm) was in front of the input beam splitter cube of the interferometer to ensure the purity of the vertical linear polarization state of the laser pulses. The optical fiber to be tested, an 82.5-cm-long birefringent HC- PCF (HC-800-02, NKT Photonics) [20] was placed in the sample arm of the interferometer. The laser pulses were coupled into the fiber by a NIR achromatic lens (L1) with a focal length of 30 mm, while the pulses coming out of the fiber were collimated by a 19.0-mm-focal-length NIR achromatic lens (L2).

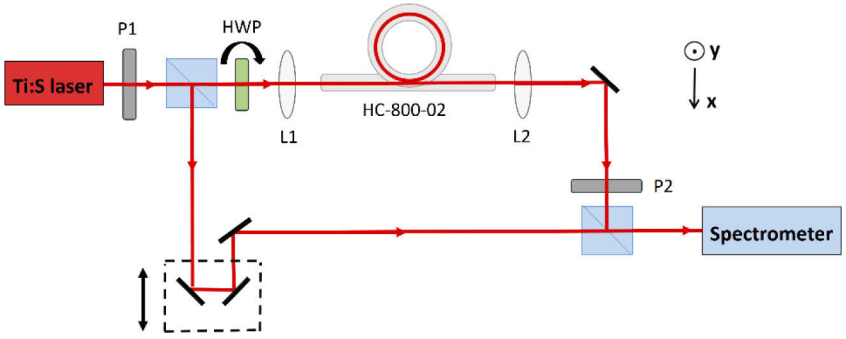

Fig. 1. Experimental setup.

The extent of the excitation of the fast and the slow polarization modes of the fiber was adjusted by an achromatic half-wave plate (HWP, spectral range: 690-1200 nm) before the fiber. Another

Optics EXPRESS

polarizer P2, similar to P1, set with vertical transmission axis, was put after the fiber in the sample arm. A delay unit used in the reference arm allows to adjust the time delay between the sample and the reference pulses.

3. Method

To determine the orientation of the principal axes of the HC-PCF spectral interferograms produced by the interference of the two sample pulses propagating along the principal axes and the reference pulses are studied. Note, that in our arrangement the orientation of the fast (β) polarization axis of the fiber is fixed to the laboratory x-y coordinate system [Fig. 2]. α denotes the angle of the polarization plane of the sample pulse to be launched into the fiber. The transmission axes of polarizers P1 and P2 were parallel to the y-axis of the coordinate system during the entire measurement. The precise adjustment of the polarization axes of the fiber was not required. However, we got interference fringes with high visibility if the angle between the transmission axes of the polarizers and one of the principal axes was about 30°-45°. The extent of the excitation of a given polarization mode depends on the angle of the polarization plane of the input sample pulse α, which can be varied by the HWP over the entire 360° range at a fixed time delay between the sample and reference pulses. Spectrally resolved interferograms were recorded at every α angle.

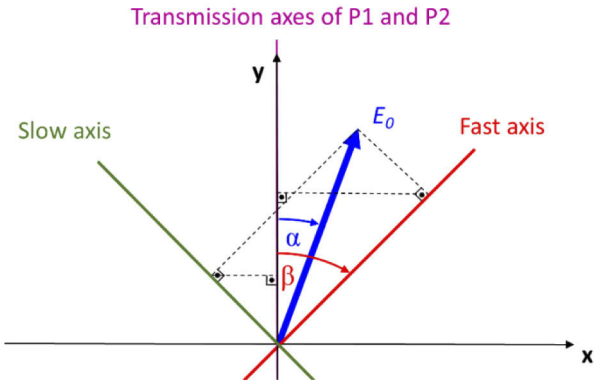

Fig. 2. Orientation of the principal axes of the HC-PCF, the polarization plane of the laser pulse to be launched into the fiber and the transmission axes of the polarizers with respect to the laboratory frame (x-y coordinate system). E_0 denotes the electric field of the sample pulse before the fiber.

In the followings we will show how the wavelength-dependent orientation of the principal axes of the fiber can be retrieved from the spectral interferograms using the WFT method. The intensity distribution of a spectral interferogram can be written as

$$\begin{aligned} I(\omega,\alpha) = I_R(\omega) + I_F(\omega,\alpha) + I_S(\omega,\alpha) + 2\sqrt{I_R(\omega)I_F(\omega,\alpha)}\cos(\phi_F(\omega)) + \\ + 2\sqrt{I_R(\omega)I_S(\omega,\alpha)}\cos(\phi_S(\omega)) + 2\sqrt{I_F(\omega,\alpha)I_S(\omega,\alpha)}\cos(\phi_{FS}(\omega)), \end{aligned} \tag{1}$$

where I_R is the intensity of the reference pulse and

$$\begin{aligned} I_F(\omega,\alpha) = C1(\omega)[1+\cos(2(\alpha-\beta(\omega)))] \\ I_S(\omega,\alpha) = C2(\omega)[1-\cos(2(\alpha-\beta(\omega)))] \end{aligned} \tag{2}$$

are the intensities of the sample pulses propagating along the fast (F) and the slow (S) axes, which are projected onto the transmission axis of P2. The functions $C1(\omega)$ and $C2(\omega)$ in Eq. (2)

Optics EXPRESS

are given as

$$\begin{aligned} C1(\omega) &= \frac{I_0(\omega)\cos^2(\beta(\omega))}{2} \\ C2(\omega) &= \frac{I_0(\omega)\sin^2(\beta(\omega))}{2}, \end{aligned} \tag{3}$$

where $I_0(\omega)$ is the intensity of the sample pulse before the fiber. The fourth and fifth terms in Eq. (1) express the interference between the reference pulse and the sample pulses propagating along the fast or the slow axis, respectively, while the last term describes the interference between the two sample pulses. ϕ_F, ϕ_S and ϕ_{FS} are the spectral phase differences between these interfering pulses.

Equation (1) can be rewritten in complex notation

$$I(\omega,\alpha) = a(\omega,\alpha) + \sum_j \left[\frac{b_j(\omega,\alpha)}{2} \exp(i\phi_j(\omega)) + \frac{b_j(\omega,\alpha)}{2} \exp(-i\phi_j(\omega)) \right], \tag{4}$$

where $j = F, S, FS$ and

$$\begin{aligned} a(\omega,\alpha) &= I_R(\omega) + I_F(\omega,\alpha) + I_S(\omega,\alpha) \\ b_F(\omega,\alpha) &= 2\sqrt{I_R(\omega) I_F(\omega,\alpha)} \\ b_S(\omega,\alpha) &= 2\sqrt{I_R(\omega) I_S(\omega,\alpha)} \\ b_{FS}(\omega,\alpha) &= 2\sqrt{I_F(\omega,\alpha) I_S(\omega,\alpha)}. \end{aligned} \tag{5}$$

As the first step of the evaluation, an inverse WFT is applied on the spectral interferogram given by Eq. (4):

$$W_I(\Omega,t,\alpha) = \int_{-\infty}^{\infty} I(\omega,\alpha) g(\omega-\Omega) \exp(i\omega t) d\omega, \tag{6}$$

where

$$g(\omega-\Omega) = \exp\left[-\left(\frac{\omega-\Omega}{\Delta\Omega} \right)^2 \right] \tag{7}$$

is a Gaussian window function, Ω is the central angular frequency and $\Delta\Omega$ is the width of the window function. Since $a(\omega,\alpha)$ in Eq. (4) is a slowly varying function of ω its inverse windowed Fourier-transform appears around $t = 0$. On the other hand, the $b_j(\omega,\alpha)$ functions, which contain the important information about the intensities of the sample pulses, change rapidly with ω and their inverse windowed Fourier-transform result in three traces on the (Ω, t) map both in the positive and the negative time domains. Considering the traces appearing only in the positive time domain, we get

$$W_I{}^+(\Omega,t,\alpha) = \sum_j \int_{-\infty}^{\infty} \frac{b_j(\omega,\alpha)}{2} g(\omega-\Omega) \exp[i\omega t - i\phi_j(\omega)] d\omega. \tag{8}$$

The width $\Delta\Omega$ of the window function should be set to meet the following two requirements: in the vicinity of Ω the amplitude of the fringes does not depend on ω

$$b_j(\omega,\alpha) \approx b_j(\Omega,\alpha) \tag{9}$$

and the spectral phase functions can be approximated by linear functions

$$\phi_j(\omega) \approx \phi_j(\Omega) + \phi_j'(\Omega)(\omega-\Omega), \tag{10}$$

where ϕ_j' denote the first derivative of the spectral phase with respect to the angular frequency ω evaluated at Ω. By performing the integrations in Eq. (8) and using approximations given by

Optics EXPRESS

Eqs. (9) and (10) we have

$$W_I{}^+(\Omega, t, \alpha) = \sum_j \frac{b_j(\Omega, \alpha)}{2} \exp[-i(\phi_j(\Omega) - \Omega t)] G_j(t - \phi'_j(\Omega)), \tag{11}$$

where $G_j(t - \phi'_j(\Omega))$ denote the Gaussian temporal envelopes of the three traces appearing in the (Ω, t) map. The ridges of the three traces are given by

$$t_{p_j}(\Omega) = \phi'_j(\Omega). \tag{12}$$

By taking the absolute square of Eq. (11) and using Eq. (12) we obtain the shape of the ridges which are formed by the intensity maxima belonging to the three traces

$$r_j(\Omega, \alpha) = |W_I{}^+(\Omega, t_{p_j}(\Omega), \alpha)|^2 = \frac{{b_j}^2(\Omega, \alpha)}{4}. \tag{13}$$

Note, that the multiplication terms having mixed indices are eliminated because the products of their $G_j(t - \phi'_j(\Omega))$ functions result in zero. Substituting Eqs. (2) and (5) into Eq. (13) yields

$$\begin{aligned} r_F(\Omega, \alpha) &= I_R(\Omega) C1(\Omega)[1 + \cos(2(\alpha - \beta(\Omega)))] \\ r_S(\Omega, \alpha) &= I_R(\Omega) C2(\Omega)[1 - \cos(2(\alpha - \beta(\Omega)))] \\ r_{FS}(\Omega, \alpha) &= C1(\Omega) C2(\Omega) \tfrac{1 - \cos(4(\alpha - \beta(\Omega)))}{2}. \end{aligned} \tag{14}$$

Equation (14) gives the intensities of the three ridges at a given Ω that change cosinusoidally with α. The initial phase angle of the cosine functions coincides with the angle of the fast principal axis of the fiber. In this way the ridges given by Eq. (14) can be used to retrieve the orientation of the principle axes. After determining the intensity of r_F or r_S ridges at every α, a cosine function fit can be used to retrieve the orientation of the principal axes at a given Ω:

$$Fit_1 = p_0[1 + \cos(2(\alpha - p_1))], \tag{15}$$

where p_0 denotes the amplitude of the cosine function and p_1 corresponds to the angle of the principal axis (β). Note, that the ridge r_{FS} can also be used to determine the orientation of the principal axes in the case when this ridge and the trace appearing at $t = 0$ do not overlap in time. In this case, the cosine function fit can be applied according to the following expression:

$$Fit_2 = \frac{p_0[1 - \cos(4(\alpha - p_1))]}{2}. \tag{16}$$

4. Experimental results and discussion

We tested our polarization alignment method on a birefringent HC-PCF. The angle α was varied in 2° steps over the range of 0-720° by rotating the achromatic HWP before the fiber by a motorized precision rotation stage. It means that 360 spectral interferograms were recorded during the measurement. This way more periods of the cosine function could be observed which resulted in better precision of the data fitting.

The steps of the evaluation method are demonstrated using three spectral interferograms recorded at specially chosen α angles. The first step of the method was to perform an inverse windowed Fourier-transform on the interferograms. We set the width of the Gaussian-window function to 8 THz, which resulted in sufficient spectral and time resolution. The WFT maps were calculated over the spectral range of the laser pulse, that is between 2.1 and 2.6 PHz. Figure 3(a) shows the first WFT map where $\alpha = 64°$. In this case we could observe only one trace, which

Optics EXPRESS

arose from the slow mode, meaning that practically only this mode was excited. At the second WFT map α was set to 109°. In this case three traces appeared. Beside the trace of the slow mode, the trace of the fast mode and a third trace, originating from the differential group delay ϕ'_{SF} (DGD), could also be observed. This shows that both polarization modes were excited to a similar extent [Fig. 3(b)]. When α = 154°[Fig. 3(c)], we could see basically one trace again, which arose from the fast mode.

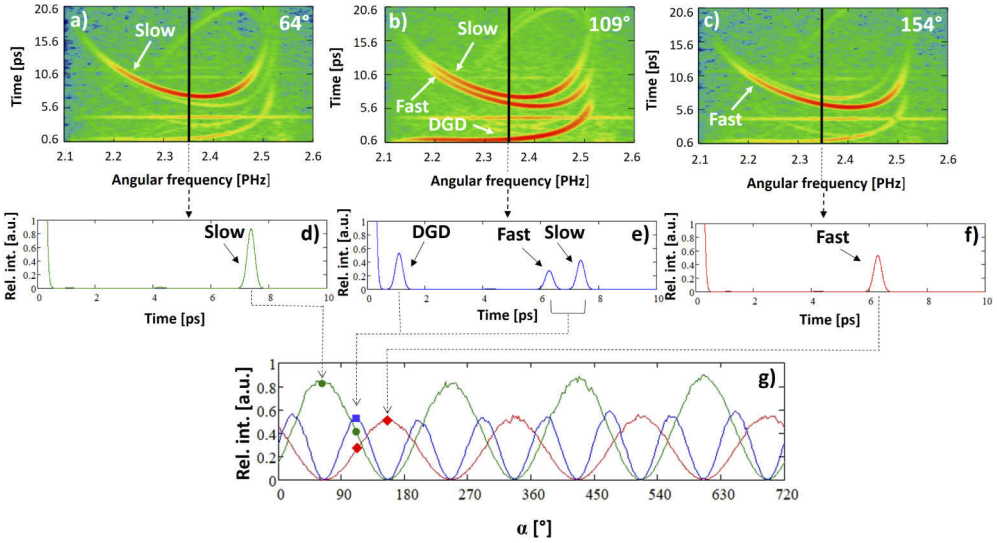

Fig. 3. WFT maps when (a) the slow mode was excited the most (α = 64°), (b) both polarization modes were excited simultaneously (α = 109°) and (c) the fast mode was excited the most (α = 154°). (d)-(f) Sections of the WFT maps taken at 2.355 PHz. (g) Relative intensities of the ridges of the slow (green curve) and the fast (red curve) modes and the DGD (blue curve) obtained at 2.355 PHz as a function of α.

The second step of the evaluation was to take a section of the WFT maps along the time axis at a given angular frequency. In our case it was chosen to be 2.355 PHz corresponding to the wavelength of 800 nm [Figs. 3(d)–3(f)]. Since the traces were well separated temporally in the selected sections, the next step was to determine their intensity maxima.

After performing these steps on all the 360 interferograms we obtained the intensities of the three ridges at a given angular frequency as a function of α [Fig. 3(g)]. The final step of the evaluation was a cosine function fit to these data according to Eqs. (15) and (16) [Fig. 4].

The orientation of a given axis was retrieved using the p_1 parameter of the cosine function fit (see Eqs. (15) and (16)). This parameter provides the angle β directly. The angles obtained for the fast axis were $\beta = 153.74 \pm 0.10°$, $\beta = 153.80 \pm 0.15°$ and $\beta = 153.65 \pm 0.03°$ from the intensity curves of the ridges belonging to the fast polarization mode, the slow polarization mode and the DGD, respectively. Note, that the precision of the measurements throughout the paper was determined by repeating the measurements more times. Since the fast and slow axes are orthogonal to each other, the angles of the slow axis are given by $\beta + 90°$.

So far, the angle β has been retrieved only at one angular frequency. However, a WFT map consists of sections belonging to multiple angular frequencies. Performing the evaluation of the WFT maps at other frequencies corresponding to the wavelength range of 762 and 830 nm, we were able to determine the dispersion of the orientation of the principal axes. As an example, in Fig. 5 we can see how β depends on the wavelength.

If the fast axis of the HWP does not have wavelength-dependence, then the wavelength-dependence of the fast and the slow polarization axes of the fiber can be determined directly by the

Optics EXPRESS

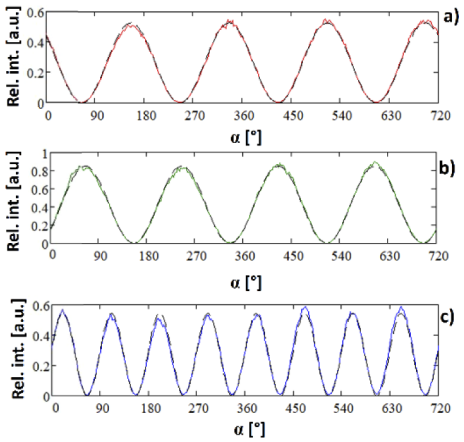

Fig. 4. Relative intensities of the ridges of (a) the fast mode (red curve), (b) the slow mode (green curve) and the DGD (blue curve) obtained at 2.355 PHz as a function of α and the fitted cosine functions (black dashed curves).

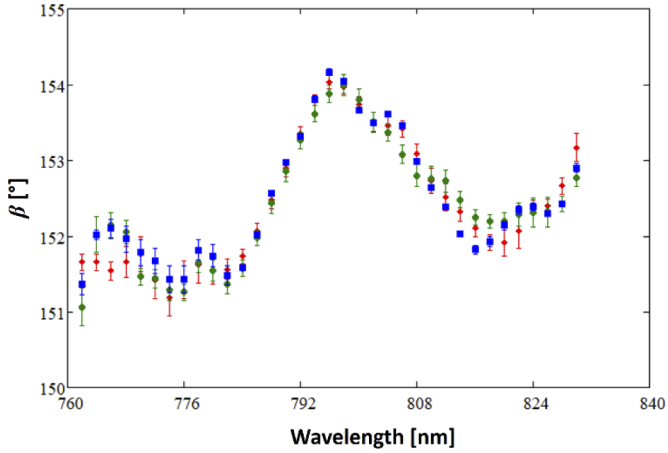

Fig. 5. Angle β as a function of wavelength obtained from the intensity of the ridges belonging to the fast mode (red symbols), the slow mode (green symbols) and the DGD (blue symbols).

presented steps of the method. To test this hypothesis, we investigated the wavelength-dependence of the fast axis azimuth angle (θ) of the HWP in two ways. Note, that θ corresponds to the angle between the fast axis of the HWP and the y-axis of the laboratory coordinate system. During these measurements, the fiber and the lenses were removed from the sample arm of the interferometer. The polarizers and the HWP remained in the same place of the setup. The transmission axes of the polarizers also remained vertical. The HWP was rotated again by 2° steps over the range of 0-720°, i.e. α was varied during these measurements. In the first case 360 spectral interferograms were recorded at every α angle while the time delay was fixed between the sample and the reference pulses. In the second case a commonly used intensity measurement method [21] was used, meaning that only the spectrum of the sample pulse was recorded at every α and the reference pulse was blocked.

The steps of the evaluation of the interferometric measurement were the same as in the case of the principal axes measurement of the fiber and the intensity changes of the ridge were obtained

Optics EXPRESS

between 762 nm and 830 nm. During the evaluation of the standard intensity measurement sections were taken from all the 360 spectra of the sample pulse in the examined wavelength range, thus, we got the intensity as a function of α at a given wavelength. In both cases, the cosine function fit was also used to retrieve the fast axis azimuth angle of the HWP. As can be seen in Fig. 6, θ shows wavelength-dependent behavior and it oscillates with an amplitude of 0.87° in the examined wavelength range, affecting the results of the principal axes measurement of the fiber. Therefore, the above obtained orientation of the fast axis of the fiber (β) must be corrected with the fast axis azimuth angle of the HWP, that is $\beta_{corr} = \beta - \theta$. The wavelength-dependence of the fast axis of the HWP is probably caused by the misalignment of the polarization axes of the crystalline quartz and the magnesium fluoride layers of the plate [22,23]. We note that a possible error source of the presented method may be the imperfect retardation of the HWP that can cause elliptic output polarization. However, the achromatic HWP used in our measurement has negligible, approximately 0.055 rad variation in the retardation in the examined wavelength range according to the manufacturer [24] in contrast to a zero-order wave plate. This small variation in the retardation has no significant effect on the retrieval of the orientation of the polarization axes of the fiber.

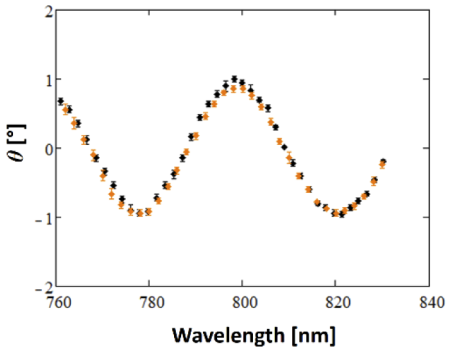

Fig. 6. Fast axis azimuth angle of the HWP as a function of wavelength retrieved from the interferometric WFT polarization alignment method (black symbols) and from the standard intensity measurement method (orange symbols).

As can be seen, the θ obtained from the interferometric WFT method and the standard intensity measurement method are in a good agreement. This means that we validated our new polarization alignment method with the standard method. The measurements of θ were repeated five times and the precision was better than 0.05°.

The corrected angles (β_{corr}) of the fast axis of the HC-PCF are depicted in Fig. 7. The angles obtained from the three ridges are in a good agreement over the scanned spectral range. We can see that the orientation of the fast axis of the HC-PCF is also wavelength-dependent and the difference between the maximal and the minimal angle of β_{corr} is about 2.3°. The principal axes measurement of the fiber was repeated five times and the precision of the method was better than 0.3°. On the edge of the examined wavelength range, which is close to the operational range of the fiber [20], the value of the error increased.

We note that temporal overlap may occur between the ridges of the polarization modes if the DGD is too small. In this case the evaluation procedure described previously cannot be performed. However, if we set the angle of the transmission axis of the second polarizer to be approximately parallel to the fast or the slow axis, we get only one ridge. Rotating the plane of the polarization of the input sample pulse over the range of 0-720° the orientation of the principal axes can be retrieved with high precision regardless of the value of the DGD.

Optics EXPRESS

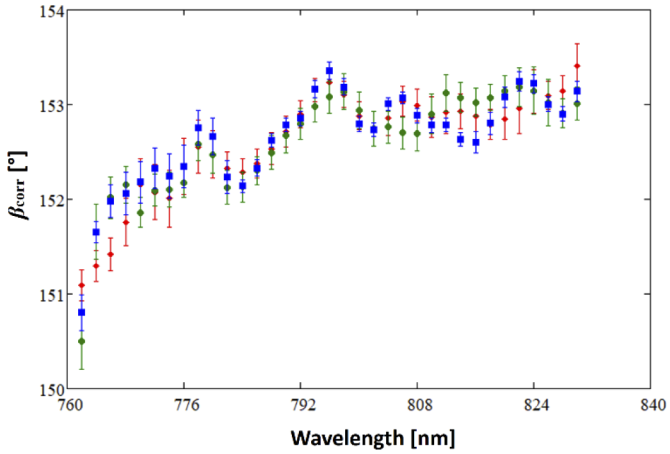

Fig. 7. Angle of the fast axis corrected with the fast axis azimuth angle of the HWP as a function of wavelength obtained from the intensity of the ridges belonging to the fast mode (red symbols), the slow mode (green symbols) and the DGD (blue symbols).

5. Conclusions

We developed a novel technique based on spectral interferometry which is suitable for determining the angles of the principal axes of birefringent fibers with high precision. Since windowed Fourier-transform is applied for evaluating the spectral interferograms, the method allows to retrieve the wavelength-dependence of the orientation of the principal axes as well. By testing this method, we showed that a commercially available, HC-PCF could also have principal axis dispersion. The precision of the wavelength-dependent angle measurement of the axes was better than 0.3°.

Our evaluation method was verified with a standard alignment method, which can be used for wave plates only.

Funding

Ministry of Human Capacities (New National Excellence Program UNKP-18-3); ELI-ALPS project, European Regional Development Fund (GINOP-2.3.6-15-2015-00001); University of Szeged Open Access Fund (4429); European Social Fund (EFOP-3.6.2-16-2017-00005).

Disclosures

The authors declare no conflicts of interest.

References

1. W. H. Cheng, C. H. Hsia, J. C. Lin, and H. M. Chen, "A simple angular alignment technique for polarization-maintaining-fiber to integrated-optic waveguide with angled interface," Mater. Chem. Phys. **50**(1), 88–90 (1997).
2. J. P. Burger, A. Ben Salem, R. Cherif, and M. Zghal, "Methodology for in situ Characterisation of a Highly Birefringent Photonic Crystal Fibre for Supercontinuum Generation," SAIEE Afr. Res. J. **103**(1), 35–40 (2012).
3. Y. Hu, J. Tan, Z. Chen, C. Zeng, S. Chang, and Z. Meng, "Phase conftast method for measurement of birefringent axes orientation of polarization-maintaining fiber," Proc. SPIE **2895**, 350–354 (1996).
4. D. Feng, Q. Fang, H. Huang, Z. Zhao, and N. Song, "Development of an embedded instrument for autofocus and polarization alignment of polarization maintaining fiber," Opt. Eng. **56**(12), 1 (2017).
5. R. H. Stolen and E. H. Turner, "Faraday rotation in highly birefringent optical fibers," Appl. Opt. **19**(6), 842–845 (1980).
6. D. de Oliveira Maionchi, W. Campos, and J. Frejlich, "Angular alignment of a polarization-maintaining optical fiber," Opt. Eng. **40**(7), 1260–1264 (2001).

Optics EXPRESS

7. N. Caponio and C. Svelto, "A Simple Angular Alignment Technique for a Polarization-Maintaining-Fiber," IEEE Photonics Technol. Lett. **6**(6), 728–729 (1994).
8. G. R. Walker and N. G. Walker, "Alignment of polarisation-maintaining fibres by temperature modulation," Electron. Lett. **23**(13), 689–691 (1987).
9. T. T. Aalto, M. Harjanne, and M. Kapulainen, "Method for the rotational alignment of polarization-maintaining optical fibers and waveguides," Opt. Eng. **42**(10), 2861 (2003).
10. O. I. Kotov, L. B. Liokumovich, A. V. Medvedev, S. I. Markov, and A. V. Khlybov, "Measuring the polarization characteristics of birefringent optical fibers using an interference technique," Tech. Phys. Lett. **30**(6), 515–517 (2004).
11. P. Arora, A. Agarwal, and A. Sen Gupta, "Simple alignment technique for polarisation maintaining fibres," Rev. Sci. Instrum. **82**(12), 125103 (2011).
12. S. L. A. Carrara, B. Y. Kim, and H. J. Shaw, "Elasto-optic alignment of birefringent axes in polarization-holding optical fiber," Opt. Lett. **11**(7), 470–472 (1986).
13. A. W. Domanski, T. R. Wolinski, and W. J. Bock, "Method for Angular Alignment of Birefringent Fibers in Fiber-optic Pressure/Strain Measurement," IEEE Trans. Instrum. Meas. **41**(6), 1050–1052 (1992).
14. Y. Ida, K. Hayhasi, M. Jinno, T. Horii, and K. Arai, "New method for polarization alignment of birefringent fiber with laser diode," Electron. Lett. **21**(1), 18–20 (1985).
15. A. Ebberg and R. Noe, "Novel high precision alignment technique for polarisation maintaining fibres using a frequency modulated tunable laser," Electron. Lett. **26**(24), 2009–2011 (1990).
16. K. Takada, K. Chida, and J. Noda, "Precise method for angular alignment of birefringent fibers based on an interferometric technique with a broadband source," Appl. Opt. **26**(15), 2979–2987 (1987).
17. P. G. Sinha, L. Bjerkan, and K. Blotekjaer, "Angular alignment of highly birefringent fibers employing acoustically scanned time-delay technique," IEEE Photonics Technol. Lett. **7**(12), 1462–1464 (1995).
18. K. Tarnowski, A. Anuszkiewicz, K. Poturaj, P. Mergo, and W. Urbanczyk, "Birefringent optical fiber with dispersive orientation of polarization axes," Opt. Express **22**(21), 25347–25353 (2014).
19. T. Grósz, M. Horváth, and A. P. Kovács, "Complete dispersion characterization of microstructured optical fibers from a single interferogram using the windowed Fourier-ridges algorithm," Opt. Express **25**(23), 28459–28468 (2017).
20. https://www.nktphotonics.com/wp-content/uploads/sites/3/2015/01/hc-800-1.pdf?1558255341.
21. W. Wang, Z. Liang, C. Li, Y. Yan, and S. Wu, "Two-intensity measurement method for determining the fast axis and phase retardation of a wave plate," in Proceedings of IEEE Symposium on Photonics and Optoelectronics (IEEE, 2012), pp. 1-4.
22. D. B. Chenault and R. A. Chipman, "Measurements of linear diattenuation and linear retardance spectra with a rotating sample spectropolarimeter," Appl. Opt. **32**(19), 3513–3519 (1993).
23. H. Gu, X. Chen, H. Jiang, C. Zhang, W. Li, and S. Liu, "Accurate alignment of optical axes of a biplate using a spectroscopic Mueller matrix ellipsometer," Appl. Opt. **55**(15), 3935–3941 (2016).
24. https://www.thorlabs.com/thorproduct.cfm?partnumber=AHWP05M-980.